Conformation of A82846B, a Glycopeptide Antibiotic, Complexed with Its Cell Wall Fragment: An Asymmetric Homodimer Determined Using NMR Spectroscopy‡

Will G. Prowse,§ Allen D. Kline,* Marshall A. Skelton, and Richard J. Loncharich

Lilly Research Laboratories, Eli Lilly and Company, Indianapolis, Indiana 46285-0403

Received March 30, 1995; Revised Manuscript Received May 24, 1995®

ABSTRACT: Proton NMR assignments were determined for the asymmetric dimer complex of A82846B with the pentapeptide cell-wall fragment. A total of 683 experimental constraints, both distance and dihedral, were collected from NOESY and COSY data sets. From these constraints, a total of 80 structures were calculated using standard X-PLOR protocols. These structures were subsequently refined using the full CHARMm potential and the addition of water molecules in the calculation. The CHARMm structures occupied more conformational space than did the X-PLOR structures and were utilized for the structure analysis. From the structures, a unique set of interactions for the dALA-5 carboxylate pocket was observed, having backbone amides from residues 2 and 3 hydrogen bonding one carboxylate oxygen while amide 4 and the side chain amide from Asn-3 hydrogen bond the other oxygen. Also, near the N-terminal region of the ligand, the GGLU-2's carboxylate forms a hydrogen bond with the asymmetric disaccharide dyad, which helps to define the interactions seen for this part of the ligand.

A82846B (Nagarajan et al., 1988; Hunt et al., 1988) is a member of a class of antibiotics whose structures are related to the glycopeptide, vancomycin (McCormick et al., 1956). The structure of A82846B is shown in Figure 1 along with the pentapeptide cell-wall fragment, Ala-GGLU-Lys-dALA-dALA.[1] Vancomycin was developed as the first glycopeptide antibiotic during the 1950's and is currently the drug of choice for treatment of infections due to methicillin-resistant *Staphylococcus aureus* and Gram-positive organisms in patients allergic to β-lactam antibiotics (Wilhelm, 1991). The mechanism of action for the glycopeptides is based upon their binding to peptides with the C-terminal motif dALA-dALA, which mimics the pentapeptide appendage of the incomplete cell wall peptidoglycan [for review, see Wright and Walsh (1992)].

From the pioneering NMR studies of Williams and coworkers during the 1980's [e.g., Williams and Butcher (1981) Williams et al. (1983), Williams (1984), and Williamson et al. (1984)], models of the cell wall peptide to glycopeptide complex were developed. NMR techniques have been used to further investigate various glycopeptide−peptide complexes (Fesik et al., 1984, 1986; Kannan et al., 1988; Waltho et al., 1988). These studies led to the proposal and subsequent refinement of a model in which complexation involves the formation of a well-defined carboxylate binding pocket by residues 1−4 of the antibiotic. The binding model is consistent with the mechanism of vancomycin resistance in the enterococci bacteria as replacement of the C-terminal dALA by D-lactic acid in the cell wall peptide eliminates one of the hydrogen bonds in the complex (Arthur & Courvalin, 1993).

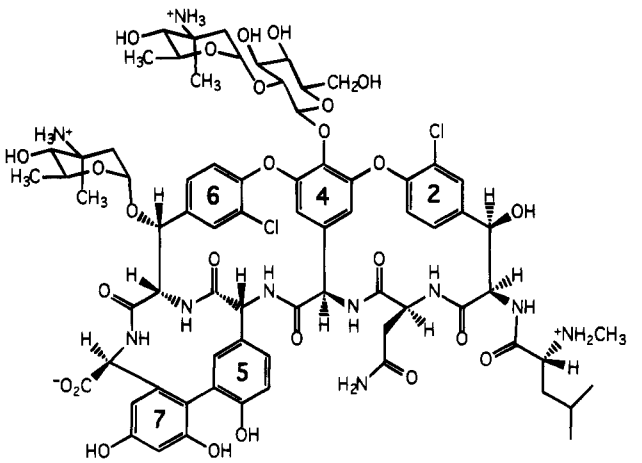

FIGURE 1: Covalent structure of A82846B (top) and its ligand peptide (bottom) indicating the appropriate stereochemistry and ionization state used in the calculations. The residue names and their sequence are shown below each molecule. Aromatic rings for A82846B are labeled with their sequence position.

‡ The coordinates have been deposited in the Brookhaven Protein Data Bank (file name 1GAC).

§ Present address: Lilly Research Centre Limited, Erl Wood Manor, Windlesham Surrey, England GU206PH.

® Abstract published in *Advance ACS Abstracts,* July 15, 1995.

[1] Abbreviations: NMR, nuclear magnetic resonance; ppm, parts per million; COSY, correlated spectroscopy; 2QF-COSY, two-quantum-filtered COSY; NOE, nuclear Overhauser effect; NOESY, NOE spectroscopy; TOCSY, total correlated spectroscopy; ROESY, rotating-frame NOE spectroscopy; EXCSY, exchange spectroscopy; RMSD, root mean square deviation; NLEU, *N*-methyl-D-leucine; HDPY, *m*-chloro-β-hydroxy-D-tyrosine; DPYG, *p*-(2-[α-4-L-*epi*-vancosaminyl]-β-1-D-glucosyl)-D-phenylglycine; DPGH, *p*-hydroxy-D-phenylglycine; HLPY, *m*-chloro-β-[β-1-(4-*epi*-vancosaminyl)]-D-tyrosine; LPGH, *m,m*-dihydroxy-L-phenylglycine; GGLU, D-γ-glutamate; dALA, D-alanine.

The binding of the rest of the cell wall peptide is less documented. Studies of the tripeptide (Lys-dALA-dALA) indicate that in aqueous solution the Lys side chain probably lies over the face of the aromatic ring of residue 7 (Williamson & Williams, 1985; Fesik et al., 1986). Comparable studies of the pentapeptide are limited, but an investigation of its interactions with aridicin aglycon (Mueller et al., 1989) used extensive NOE data and distance geometry to generate models of the complex. The Lys side chain was again found to lie over ring 7, but contrary to previous studies [e.g., Williamson et al. (1984)] a hydrogen bond involving the Lys carbonyl and amide 7 was not evident from ^{1}H and ^{15}N chemical shift comparisons between signals of the free and bound states of the glycopeptide. The NOE data for the pentapeptide (Mueller et al., 1989) also indicated certain conformational preferences for the GGLU residue, with NOE's being observed to aromatic protons on ring 6.

The dimerization of vancomycin was discovered a number of years ago by Nieto and Perkins (1971), though its structural basis was determined more recently by Williams and co-workers (Waltho & Williams, 1989). They have subsequently characterized the key features that promote dimerization for a number of glycopeptides, including A82846B (Gerhard et al., 1993; Groves et al., 1994a; Mackay et al., 1994a,b). The dimer surface consists of hydrophobic interactions between aromatic rings 4 and 6 and a series of six hydrogen bonds mostly between the opposing backbones. Recently, the eremomycin−(pyrrole-2-carboxylate) dimer complex has been identified as asymmetric due to differences in the disaccharide orientations (Groves et al., 1994a). An X-ray structure of a related glycopeptide showed that the unligated dimer can also be asymmetric (Sheldrick et al., 1995). The biological significance of dimerization is at this time unclear, although some (Gerhard et al. 1993; Mackay et al., 1994b; Beauregard et al., 1995) have speculated that it may play an active part in the antibacterial action of glycopeptides. In this report, the asymmetric dimer complex of A82846B with its pentapeptide ligand is examined, with particular attention given to the ligand−glycopeptide interactions.

MATERIALS AND METHODS

The sample of A82846B used in these studies was isolated and purified from *Amycolatopsis orientalis* NRRL 18090 (Nagarajan *et al.*, 1989). The pentapeptide, Ala-GGLU-Lys-dALA-dALA, was purchased from Sigma Chemical Co. (St. Louis, MO). Both samples were used without further purification. NMR samples of the A82846B−pentapeptide complex were prepared mixing equimolar amounts of A82846B and pentapeptide into either $^{2}H_2O$ or 9:1 H_2O/$^{2}H_2O$, and the pH was adjusted by small additions of HCl or NaOH, monitored by a pH meter. Final concentrations were between 5 and 7 mM. $^{2}H_2O$ samples were lyophilized and dissolved back into $^{2}H_2O$. The pH was monitored before and after lyophilization. Amide proton exchange samples were prepared by mixing A82846B and pentapeptide in water and adjusting the pH to 3.5. The sample was lyophilized, dissolved in $^{2}H_2O$, and inserted into the spectrometer set to 10.0 °C.

All NMR experiments were carried out on a Varian Unity 500 MHz spectrometer. Probe temperatures were regulated with a large volume solvent bath: 10.0 °C for assignment data, 0.5 °C for NOE constraints, and 20.0 °C for chemical exchange spectra. Presaturation was used to suppress the solvent signal. NOESY (Bodenhausen et al., 1984), ROESY (Rance, 1987), TOCSY (Braunschweiler & Ernst, 1983; Rucker & Shaka, 1989), and 2QF-COSY (Rance et al., 1983) were collected on all samples while HMQC (Bax & Subramanian, 1986) and EXCSY (Fejzo et al., 1990) were collected only on $^{2}H_2O$ samples. Data were processed and analyzed on Silicon Graphics workstations using the Felix software package (version 2.35; Biosym Technologies, Inc.). NOESY (60 ms) cross peaks were classified as strong, medium, or weak and assigned upper limits of 2.50, 3.50, or 5.00 Å with the lower bound set to 1.80 Å (Wüthrich, 1986). Hydrogen bond constraints were enforced between amide proton and oxygen (2.00 ± 0.20 Å) and between amide nitrogen and oxygen (3.00 ± 0.20 Å). Increased lower bound constraints were determined using Felix-Model (Biosym Technologies, Inc.) and initial calculated structures; for these cases, lower bounds were set to 3.00 Å; upper bounds were set to 10.00 Å (for a few cases a weak NOE was observed, so the upper limit was set to 5.00 Å). Scalar coupling values were measured using the multiplet structure for 2QF-COSY cross peaks and torsion ranges were set to established values (Wüthrich, 1986).

Structure calculations were performed with the program X-PLOR 3.1 (Brünger, 1992) running on a CRAY-2S/128 supercomputer. CHARMm/X-PLOR topology files were created for the glycopeptide's nonstandard amino acid residues and are given as supplementary information. Input files were created by the QUANTA program (version 4.1; Molecular Simulations, Inc.) and included distance geometry, followed by 10 000 ps of high temperature (1000 K) simulated annealing, 8000 ps of cooling to 300 K, followed by 5000 ps of room temperature dynamics, and finally 5000 steps of minimization. The refinement procedure utilized the CHARMm program (version 2.3; Molecular Simulations, Inc.) with standard input files created by Quanta. The explicit hydrogen bond constraints, used in the X-PLOR calculations, were removed, and dihedral constraint ranges were replaced with the average angle values from the X-PLOR structures with a force constant of 10. X-PLOR structures were solvated with a 10 Å layer of water molecules and then subjected to 500 steps of minimization, 1200 steps of heating to 300 K, followed by 10 ps of equilibrium dynamics (300K), and finally 3000 steps of minimization. Structure analysis, RMSD calculations, and diagrams were done using the QUANTA program.

RESULTS AND DISCUSSION

Resonance Assignments. The ^{1}H NMR spectrum of the A82846B−pentapeptide complex showed many paired resonances, consistent with the formation of an asymmetric dimer (Gerhard et al., 1993; Groves et al., 1994a). In addition, ROESY spectra revealed that the two sets of signals were in chemical exchange, again congruent with the interconversion seen between forms (Waltho & Williams, 1989; Groves et al., 1994a). At the time this work was started, it was not known that these dimers were asymmetric. It is now clear that the same conclusions can be drawn for the A82846B−pentapeptide as for the eremomycin−(pyrrole-2-carboxylate) complex.

The NMR assignment of this asymmetric complex required that each resonance be assigned not only to a specific proton

in the glycopeptide or ligand but also to one of the two dimer segments (designated segment A or segment B). To minimize exchange cross peaks in TOCSY and NOESY spectra, temperatures were reduced to 10 °C or lower. Higher temperatures were only used to induce exchange for the EXCSY spectra, when signal pairing provided a form of spectral cross-check.

The assignment procedure used was based on the classical method for homonuclear assignments (Wüthrich, 1986). Initially COSY, TOCSY, and HMQC experiments were used to identify discrete groups of resonances associated with individual amino acids, aromatic rings, or sugars for both A82846B and the pentapeptide ligand. Next, NOESY spectra were used to establish which groups of resonances were covalently linked by assessing the number and intensity of NOE's between units.

Using COSY and TOCSY data alone, it was possible to assign all of the protons into discrete peptide or sugar residues. Particularly helpful in this regard were the sighting of numerous four-bond correlations within aromatic rings and from aromatic rings to backbone. This allowed for nearly all of the peptido-protons, from amide to side chain, to be grouped into amino acid spin systems without depending on NOE's. The only exceptions were the backbone−aromatic connections for HDPY-2 and DPYG-4 which had to be established by NOE.

The assignments of the sugar protons were made in a similar manner. The anomeric protons were identified on the basis of the distinctive ^{13}C shift of their anomeric carbons. The COSY spectrum was then used to assign complete sets of protons for two glucose residues. For the vancosamine units, complete COSY/TOCSY connections were not possible due to break in the proton scalar coupling network at C3. Four fragments, corresponding to CH-CH_2-C-CH_3, were found in the COSY spectrum, including a four-bond correlation between the methylene and the methyl group. The CH frequency corresponded to the characteristic anomeric ^{13}C shift and identified the signals as C1, C2, and C3. In addition, four separate CH-CH-CH_3 fragments were found in the COSY spectrum and corresponded to C4, C5, and C6. The four CH-CH_2-C-CH_3 fragments were linked exclusively to their corresponding CH-CH-CH_3 fragments via intense and resolved NOE peaks (Figure 2) between the axial C3 methyl group and the axial proton at C5. These connected spin groups were assigned as part of the same sugar ring. The EXCSY spectrum linked the A/B pairs and provided an added confirmation of the vancosamine assignments.

At this stage there were two sets of spin fragments for each of the 12 peptide residues and three sugar residues. NOE's were used to identify the peptide sequence for both the ligand and glycopeptide in the two conformations. Figure 3 shows the results for the sequential assignments. Uninterrupted connections were identified in the spectra along all the peptide chains, attesting to the quality of the data. An unusual set of connections (indicated by the asterisk) was observed for DPHG-5 and HLPY-6 in the glycopeptide. Amide proton signals for HLPY-6 gave no NOE's to the preceding residue, but its α protons did show NOE's. This agrees with early work (Sheldrick et al., 1978; Wüthrich, 1986) that indicates a *cis* amide bond between these residues in this type of glycopeptide.

The final step in the assignment procedure used NOE's from the sugar protons to determine their covalent attachment. For both HLPY-6 vancosamines, anomeric protons had NOE's with $C^{\beta}H$ and $C^{\delta}H^1$, allowing for an unambiguous assignment. The remaining vancosamines showed NOE's from their anomeric proton to the C2 proton of the proceeding glucose. Numerous other NOE's were detected between these two sets of rings in the disaccharide unit which confirmed these assignments. The weakest assignment connection occurs between the glucose sugar and its aromatic rings. This difficulty was caused by a lack of aromatic protons at the sugar attachment site. Despite this, segment B's C1 proton has a weak NOE with DPYG-4 $C^{\delta}H^1$ ring proton. In addition, both of these protons share medium sized NOE's with HDPY-2 $C^{\epsilon}H^1$. For the remaining glucose no detectable cross peaks were observed to any of segment A's ring protons. However, the same protons (DPYG-4 $C^{\delta}H^1$ and HDPY-2 $C^{\epsilon}H^1$) which had shown connections to the glucose in segment B have NOE's to the vancosamine C5

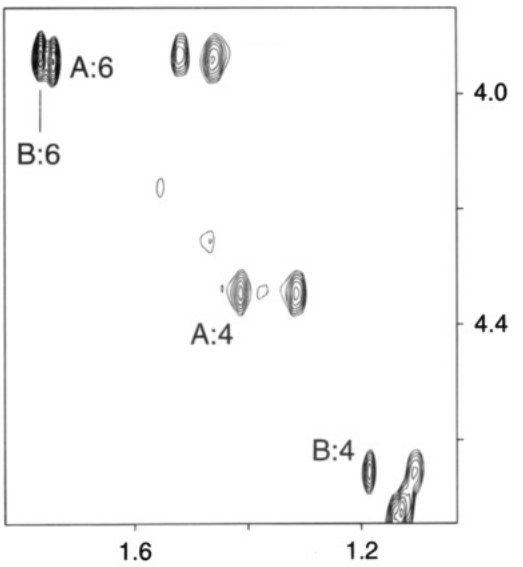

FIGURE 2: Portion of the NOESY spectrum (^2H_2O, 0.5 °C) for the A82846B−pentapeptide complex showing the connections between the two halves of the vancosamine ring. The four cross peaks connecting the C3 methyl (horizontal axis) with the C5 proton (vertical axis) are labeled with segment and glycopeptide residue number. The scale on both axes is in ppm.

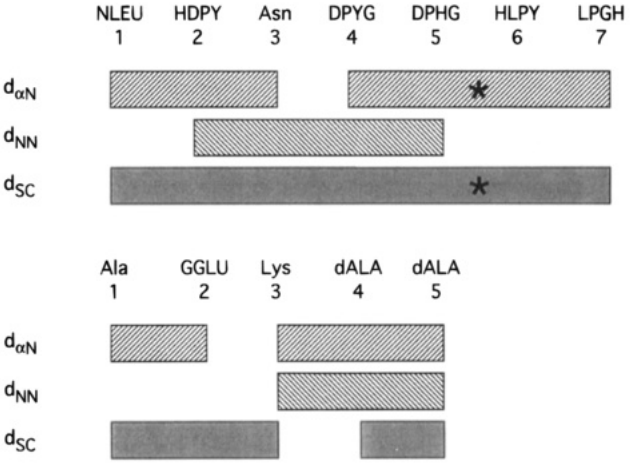

FIGURE 3: Summary of the sequential NOE's for segment A of the A82846B−pentapeptide complex (segment B had identical linkages). $d_{\alpha N}$ and d_{NN} had their standard meanings (Wüthrich, 1986). d_{SC} indicates amide protons that had NOE's to any of the preceding residue's side chain protons. The connections made through the $C^{\alpha}H$ rather than the NH are indicated with an asterisk.

Table 1: Summary of NOE Violation Statistics for the 80 X-PLOR and CHARMm Structures[a]

	number of violations	largest violation (Å)	sum of the violations (Å)
X-PLOR	61−77	0.16−0.34	3.14−5.07
	67 ± 3	0.26 ± 0.06	3.95 ± 0.33
CHARMm	53−81	0.19−0.53	4.02−6.03
	64 ± 4	0.27 ± 0.06	4.89 ± 0.46

[a] Range of values are given in the upper entry, and the mean and standard deviation are given below.

and C6 protons in segment A, providing evidence for the identification of the final disaccharide. The list of proton chemical shifts for A82846B-pentapeptide complex is given as Table 1 in the supplementary information.

The largest chemical shift differences between segment A and B occur for the disaccharides. These results are consistent with published observations (Waltho & Williams, 1989) and with the disaccharide orientation being responsible for the asymmetry of the complex (Groves et al., 1994a). Additional shift differences between the A and B occur at the GGLU residue, suggesting that this part of the pentapeptide is near the disaccharides. With the assignments complete, the final goal of this paper is to determine the conformation of this asymmetrical dimer.

NOE Assignments and Distance Constraints. To carry out structure calculations, a full assignment of both the H_2O and ^2H_2O NOESY spectra was required to characterize the dimer interface and the ligand binding sites. Because of exchange complication in the NOESY data, temperatures were lowered to 0.5 °C and mixing times were kept short (60 ms), thereby removing this interference.

The initial assignment of the NOESY spectra provided 350 distance constraints. Overlapping cross peaks and peaks with ambiguous assignment were not included at this stage. Structure calculations produced a family of 20 structures consistent with the NOE constraints. These structures were used to help assign additional cross peaks, expanding the constraint list to 581. A set of 32 structures was calculated, resulting in 16 structures consistent with the new constraints. These structures were used in an iterative fashion to produce stereospecific assignments and a group of lower bound constraints.

Stereospecific assignments were accomplished for the vancosamine C2 protons, for NLEU-1 β protons and its δ methyls, and for Lys-3 and GGLU-2 β and γ protons. In all cases assignments were obtained for both the A and B segments. The sugar protons were assigned using the observed chair conformation and the anomeric J-couplings. The other stereospecific assignments were gained by examination of the differential NOE intensities for the proton pair, then comparing to the structural preferences seen in the generated structures. To push the identification process, a pair of constraints from a neighboring proton to the prochiral signals that fell into the same intensity classification but yet had different NOE intensities were differentiated modestly by the addition or subtraction of 0.50 Å from the upper limit. The number of stereospecific assignments, particularly for Lys-3 and GGLU-2, reflects the degree of conformation this complex has.

In these 16 structures, two distinct conformers were observed for both the dALA-5 carboxylate and amide between Asn-3 and DPYG-4. The conformers for dALA-5 had their carboxylates either in or out of the binding pocket, while the amide conformers had their protons either pointing toward the binding pocket or toward the dimer interface. Since both sets of conformers showed minimal deviation within their respective families, it was decided to calculate the NOE intensities for the amide protons associated with the binding pocket. The conformers having their carboxylate or amide in the pocket had calculated NOE's that were consistent with experimental spectra, while those NOE's from conformers out of the pocket were not. To suppress the generation of inconsistent conformers, proton pairs that had large calculated NOE intensities yet were weak or nonexistent in the NOESY spectrum, received a lower limit constraints of 3.00 Å. The number of these constraints for both A and B segments totaled 33.

Dihedral angle constraints were established whenever proton J-coupling constants had large or small values. In all, 30 constraints were determined, most for the six sugar rings in the complex. In conjunction with the stereospecific assignments, dihedral constraints were determined for glycopeptide NLEU-1 χ_1 angle and the ligand's Lys-3 (ϕ and χ_1) and GGLU-2 (ϕ, χ_1, and χ_2).

Twelve slowly exchanging amide protons were discovered when the preformed complex and dissolved into ^2H_2O (Wagner & Wüthrich, 1982). Assignments were verified by examination of a TOCSY acquired during the exchange period. The amide signals still present after 3 h were (both segments A and B) DPYG-4, DPHG-5, HLPY-6, and LPGH-7 from the glycopeptide and Lys-3 and dALA-5 from the ligand. Hydrogen acceptors for these amides were determined by examining the initial 20 structures. For 10 of these amide protons, unique acceptors were found, so a constraint was produced. But for the amides at DPYG-4 the situation was complicated due to the presence of two oxygen acceptors from the dALA-5 carboxylate, and no hydrogen bond constraint was ever enforced on this amide. The final constraints came from the observation of the amino protons for HLPY-6 vancosamine, which would normally be in fast exchange and not detected. The close proximity of HDPY-2 carbonyl oxygen in the structures made it likely that hydrogen bonding is the reason the amino signal is observed. All of the hydrogen bonds detected here, except for Lys-3 HN to LPGH-7 CO_2, have been reported (Waltho & Williams, 1989).

For the final set of calculations, the constraint list contained 631 distance constraints from NOESY spectra, 22 distance constraints for hydrogen bonds (X-PLOR only), and 30 dihedral constraints. Of the NOE constraints, 347 occur within glycopeptides, 71 occur within the ligands, 80 occur between the two glycopeptides, and 133 occur between ligand and glycopeptide. The 683 total constraints gives a constraint density of greater than 28 per residue, which is high for NMR structure calculations (Clore & Gorenborn, 1993). A list of the distance constraints is given as Table 2 in the supplementary information.

Structure Calculations. A group of 80 structures were generated using the X-PLOR protocol and the NOE, hydrogen bond, and dihedral angle constraint lists. The entire set of structures was fitted to the average structure, and this is shown in the top half of Figure 4. The dimer complex is shown from its symmetrical side (away from the disaccharides) with the peptide ligands located to the right and left. In the bottom half of Figure 4, the same 80 structures are

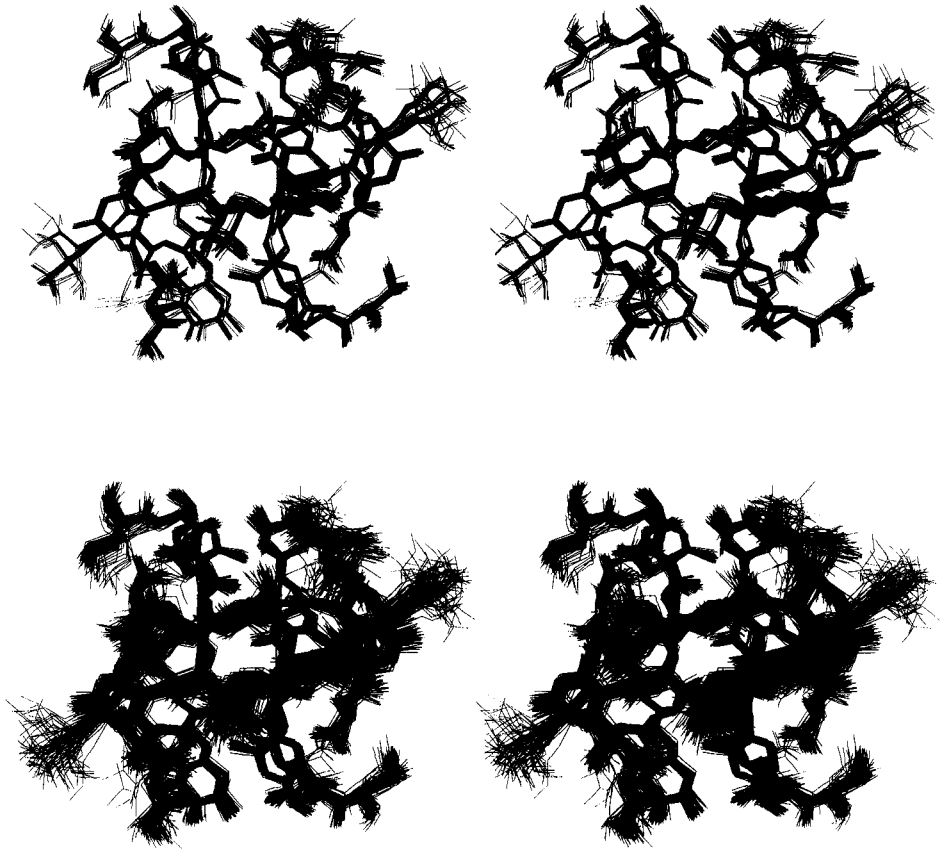

FIGURE 4: Stereodiagram of the entire ensemble of 80 X-PLOR (top) and 80 CHARMm (bottom) structures viewed along its pseudo 2-fold axis. Only heavy atoms of the glycopeptide−peptide complex are displayed. Structures were best fit to an average structure using the 94 "core" atoms.

shown after refinement using the CHARMm protocol described in Materials and Methods. Subsequently, the two sets of structures will be referred to as either X-PLOR or CHARMm structures.

Central to any NMR structure calculation is how well do the structures satisfy the experimental constraints. A summary of the NOE violations is shown in Table 1 with the results depicted as both a range and mean value. The total number of violations for both the X-PLOR and CHARMm structures is around 10%, and the largest violations seen for each of the X-PLOR and CHARMm structures is generally less than 0.30 Å, well within expected errors for NOE data. The sum total of NOE violations for each structure shows that the average violation to be under 0.10 Å. While the CHARMm structures have a slightly elevated violation sum, both sets of structures comply with the experimental constraints.

Another consideration is how well the coordinates fit standard energy functions. In that regard, it is possible to identify misfolded or trapped conformations by their unusual energy values. The energy distributions (not shown) for both the X-PLOR and CHARMm structures were tightly clustered, having no outlying points. The distributions confirm that both are reasonable solutions to the experimental constraints and similar in response to the energy function, and so no structures were eliminated from these calculations.

The way that the CHARMm energy function was used in this study represents a more complete set of molecular forces and is therefore a better test of acceptability for the two sets of structures. When comparing the CHARMm energy for the corresponding X-PLOR and CHARMm structures, the average energy reduction was 470 kcal/mol for the latter. Optimizations of van der Waals and electrostatic interactions caused this reduction. While both series satisfy experimental constraints, the CHARMm set better satisfies standard energy functions (Brooks et al., 1983).

A sense of precision can be obtained by calculating RMSD's on the 80 structures. Ninety-four of the best defined atoms from the core of the complex were chosen from the 222 heavy atoms in the entire structure. These atoms were taken from both glycopeptide backbones for residues 2−7 and the aromatic rings for residues 2, 4, and 6. The RMSD's for the "core" atoms are 0.14 ± 0.05 Å for the X-PLOR and 0.24 ± 0.05 Å for the CHARMm structures. The low average RMSD is due in part to the covalently constrained nature of these glycopeptides, but the high density of NOE constraints also contributes significantly to the level of definition (Clore & Gronenborn, 1993). The inclusion of all heavy atoms increases the RMSD to 0.57 ± 0.10 and 0.70 ± 0.08 Å, respectively, as a result of regions that have few NOE's and were poorly determined.

The RMSD's for the CHARMm structures were expected to be lower than the X-PLOR structures due to additional energy terms. However, for the core atoms they were nearly doubled for the CHARMm structures. The higher deviations can also be seen in the ensemble view of Figure 4. The reason for the expansion in the CHARMm calculations might be related to the removal of specifically assigned hydrogen bonds from the distance constraint list. However, this seems unlikely as a repeat of the X-PLOR calculations without these hydrogen bond constraints did not increase the RMSD of the core atoms. The reason for the expansion into previously

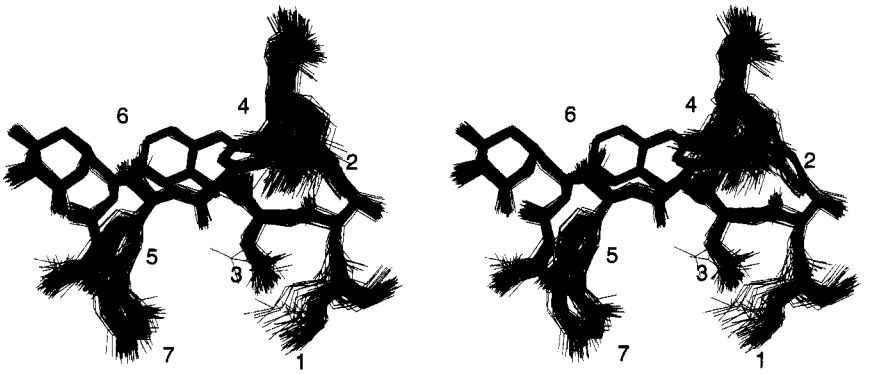

FIGURE 5: Stereodiagram of segment's A glycopeptide using the same fit shown in Figure 3. Side chain position is marked with the residue number.

Table 2: Average RMSD's for the 80 Structures for Various Subsets of the Glycopeptide with Respect to the Central Core Atoms[a]

region added to "core"	none	side chain (1,3)	side chain (5,7)	disaccharide (4)
number of atoms	94	116	124	134
average RMSD (Å)	0.24	0.36	0.30	0.35
standard deviation (Å)	0.05	0.10	0.06	0.07

[a] Numbers in parentheses indicate the residue number of the atoms being added.

disallowed areas must be due to the addition of attractive potentials within the CHARMm calculations. The simplified X-PLOR energy function evidently removes regions of allowed space by its use of hard sphere potentials. These results suggest, therefore, that the use of a full potential function is necessary, particularly when the RMSD values approach 0.30 Å.

While the refinement of the X-PLOR structures through CHARMm did create additional allowed regions, no significant structural transitions occurred between the calculations. The only exception was at the dALA-5 binding pocket where a series of shifts was observed. This region will be addressed in a later section.

Structure Analysis. Because of its improved energy values and expanded conformational space, the structural analysis will be done using the set of CHARMm structures, unless otherwise stated. The analysis will be divided into three parts: (i) discussion of the glycopeptide monomer unit, (ii) analysis of the dimer interface, (iii) the interactions between the peptide ligand and the glycopeptide.

To visualize the definition of the monomer, the glycopeptide segment A (for this analysis segments A and B are similar) is displayed in Figure 5. Excellent resolution of the three linked aromatic rings, the HLPY-6 vancosamine and the associated backbone atoms is apparent. These atoms are the most buried from solvent and are referred to as the "core" subset of atoms.

The dALA-5 carboxylate binding pocket is formed by two sets of side chains: the linked aromatic rings at 2 and 4 and the side chains of NLEU-1 and Asn-3. The side chains of 1 and 3 have almost unique conformations, throughout the 80 structures. However, while the dihedral angles fall into single wells, the definition of the atomic position is not as good as the core atoms (Figure 5). This can also be seen in Table 2 where the heavy atoms of NLEU-1 and Asn-3 increase the RMSD. Some of the increased variation probably results from solvent exposure, but the definition of these surface groups is consistent with their importance to biological activity (Nagarajan, 1993).

The covalently linked aromatic rings at residues 5 and 7 form a wall in the binding pocket which helps to turn the ligand toward the disaccharide region of the dimer. The side view of these rings in Figure 5 emphasizes the spatial variations. Table 2 shows that the increase in RMSD upon adding them to the core is smaller than that for adding the NLEU-1 and Asn-3 side chains.

The DPYG-4 disaccharide produces the asymmetry seen for the dimer complex (Groves et al., 1994a). This disaccharide has a unique conformation (Figure 5) though its definition decreases further out the chain. The addition of the disaccharide to the core atoms significantly increases the RMSD (Table 2). The interactions which the disaccharides form in the dimer and with the ligands will be discussed later.

The dimer interface for A82846B is shown in Figure 6 and appears to be identical to the Groves conformation. The present structures, however, are based on far more NOE constraints (667 versus 58) which produces a more precise structure. Eighty independent structures have been calculated in an effort to fully characterize allowed conformational space. The results from the structural analysis not only concur that the features observed for eremomycin (Groves et al., 1994a) exist in A82846B but that they are required by the NMR data. That is to say, deviations from these features are not significantly populated.

Groves et al. (1994a) also showed that the disaccharides cause the asymmetry found in the dimer complex by forming a tight head-to-head arrangement. They illustrated the packing of the disaccharides for eremomycin and reported a hydrogen bond across the dimer interface between segment A glucose C3-OH and segment B vancosamine ether oxygen. Since A82846B has the same disaccharides, a similar conformation was expected. This region is shown in Figure 7, matched to the Groves orientation. The A82846B conformation is qualitatively similar, though the structures differ in one important aspect; the hydrogen bond they reported does not occur in any of these structures. Careful examination indicates that the glucose C3 C-O bond is further from the oxygen and pointing in the opposite direction compared to the published structure. Though hydrogen bonds are occasionally formed between the disaccharides, none were consistently found, minimizing the importance of hydrogen bonding to maintaining the dimer in this region.

A detailed understanding of the asymmetry observed in the A82846B−pentapeptide complex can be gained by

FIGURE 6: Stereodiagram displaying the dimer interface, made up of the "core" atoms. This is a subset of the atoms used in Figure 3. Segment A is on the left side; the sugar ring shown is the monosaccharide from HLPY-6.

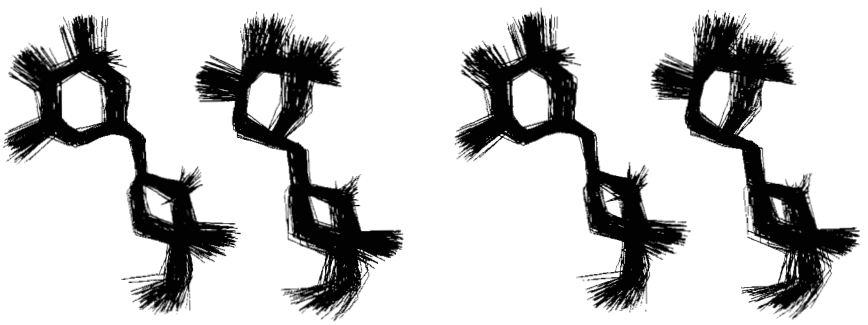

FIGURE 7: Stereodiagram of the disaccharides for both segment A (left) and B. The fit was done to an average structure using only the 24 ring atoms and the two interconnecting atoms. Orientation is similar to that shown in Groves et al. (1994a).

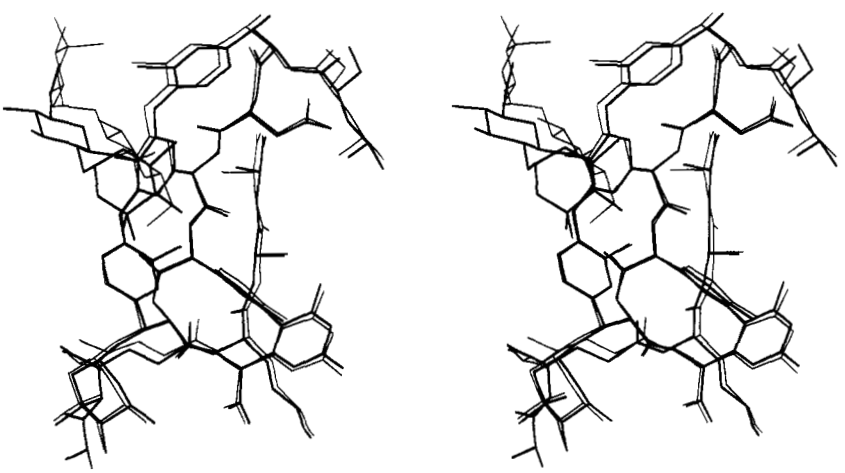

FIGURE 8: Stereodiagram showing the asymmetry of the two halves of the dimer complex. In the thick line is shown the average structure for segment A used to fit the ensemble in Figure 3. In thin line is the same for segment B. Both averages were superimposed using the glycopeptide backbone atoms from residue 2 to 7 and using the saccharide and aromatic ring atoms from HLPY-6. The structures are geometrical averages which can be highly distorted from standard covalent arrangements (note dALA-5 carboxylate at binding pocket).

superimposing the A and B segments (Figure 8). The most prominent change is the 180° rotation of the dihedral angle connecting the disaccharide to ring 4. The other changes are smaller and are related to this rotation. For example, the divergence of ring 2 and the dALA-5 methyl group is explained as they are in direct contact with the disaccharides, and these differences are also transmitted to the rest of the binding pocket. The other deviations occur at the ligand N-terminus where Ala-1 and GGLU-2 take drastically different paths. Both ligand termini will be discussed later.

The static image of the A and B segments in Figure 8 is not a complete picture of what occurs in solution. As was

pointed out (Waltho & Williams, 1989), there is an exchange process between the two states with a measured rate of ~8 Hz for the ristocetin−tripeptide complex. This exchange behavior was also evident for the A82846B−pentapeptide complex, measuring 2 Hz at 20 °C. The slower rate is reasonable given its higher dimerization constant and larger ligand (Mackay et al., 1994b). To understand the nature of the conformational transition, efforts were made to simply rotate the disaccharide dihedral angles in such a way as to avoid severe van der Waals contacts, which turned out to be impossible. It seems probable that the exchange between A and B takes place in the monomeric form. Presuming that bond rotation of the sugar−aromatic ring is much faster than reforming the dimer, the observed rate constant represents the rate of dissociation of the dimer. To test this explanation, additional studies need to be done to show that this is a first-order rate constant. Also it would be interesting to repeat the amide exchange study (Mackay et al., 1993) at a higher pH where EX1 kinetics might occur. This could then give a second independent measure of the dimer dissociation.

The antibiotic activity of these glycopeptides is the result of binding cell wall appendages ending in dALA-dALA (Williams & Butcher, 1981; Williams et al., 1983; Fesik et al., 1986; Mueller et al., 1989). Thus, an understanding of how these peptide ligands bind is central to a knowledge of how the antibiotic works. Many aspects of this binding have been revealed by the pioneering work of Williams and his co-workers (Williams, 1984); however, many questions still remain. For example, the critical recognition of the dALA-5 carboxylate is normally drawn as three hydrogen bonds from amides 2, 3, and 4 with little documentation as to the specific identity and positioning of these bonds. The present study addresses this issue and helps define the essential hydrogen bonds. A further question is the role the N-terminal region of the peptide plays in ligand binding. Most studies to date have used the shorter di- and tripeptides, based on evidence that the monomeric glycopeptide principally recognizes the dALA-dALA and not the rest of the cell wall peptide. In contrast, the A82846B dimer has specific interactions beyond dALA-dALA.

Analysis of the structures confirms the glycopeptide binding pocket seen for the dALA-5 carboxylate. For segment B and for nearly all of segment A, the ligand's carboxylate is buried as expected in a ring of amide protons from residues 2, 3, and 4. However, six of 80 segment A structures had their carboxylates out of this pocket, interacting instead with the disaccharides. While the NOE violations are slightly higher for these structures, the violations were not so high as to render this conformation spurious. The data clearly allow for the possibility of having the carboxylate out of the pocket, but at best this should be considered only a minor conformer. For subsequent discussions of this site, these six structures will be ignored.

The location of the carboxylate oxygens with respect to the glycopeptide's proton donors is illustrated in Figure 9 for both the X-PLOR and CHARMm structures. The figure shows three approximate oxygen positions corresponding roughly to the apices of a triangle. Though the populations of the positions vary from A to B and from X-PLOR to CHARMm, their presence is common to all. Three of the four proton donors shown have been identified (Williams, 1984; Groves et al., 1994a) as participating in carboxylate binding. But while the biological importance of the Asn-3 side chain has been established (Nagarajan, 1993), no structural role for this group has ever been identified. These calculations point to this side chain as being an integral part of the hydrogen-bonding network for recognition of the carboxylate.

The hydrogen donation to each of the three oxygen positions is unique. For the X-PLOR structures the donor−acceptor identity is consistent and unambiguous, while for the CHARMm structures it is related, though clearly shifted. The lowest apex in the oxygen triangle will be defined as position 1. At this site the oxygen rests in a crevice formed by rings 2 and 4, being hydrogen bonded by backbone amides 2 and 3 (Figure 9A,B). Oxygen position 2 is the upper right apex and is spatially less restricted than position 1. The hydrogen donors for this position are the backbone amide at residue 4 and the side chain amide from residue 3. Finally, position 3 is only occasionally seen for the X-PLOR structures and places the oxygen away from the influence of amides 3 and 4 and the side chain asparagine, though still within hydrogen bonding distance of amide 2. Results from the X-PLOR calculations indicate that the predominant structure have amides 2 and 3 hydrogen bonding the oxygen at position 1 while amide 4 and the side chain amide share the oxygen at position 2. This scheme will be referred to as 23-4N.

The refinement of the X-PLOR structures using the CHARMm procedure modified the carboxylate binding due to the inclusion of the electrostatic energy function and the addition of water molecules. First, as was noted earlier, the space occupied by all the atoms is larger for the CHARMm structures (Figure 9C,D). Second, the population of oxygen position 3 increases for both segments A and B. This is consistent with the presence of solvent in the calculation which is capable of hydrogen donation to the oxygen only when it occupies position 3. The 23-4N network can still be observed, though, the backbone amides all shift toward intermediate positions where they can hydrogen bond simultaneously to both oxygen positions 1 and 2. This shifting from linear to split hydrogen bonds may well be artifactual and caused by the charge parameters and the assumption of constant dielectric in the CHARMm calculations (Brooks et al., 1983; Bernard Brooks, personal communication). Regardless of the accuracy of the electrostatic potentials, the presence of the 23-4N pattern for both sets of structures is evidence of its importance to ligand binding.

This hydrogen bonding pattern has some similarity to the scheme reported earlier (Williams, 1984) which was developed from CPK models. In their model, amide 2 and amide 4 hydrogen bond to different oxygens on the carboxylate, agreeing with the 23-4N pattern found for A82846B. However, earlier reports indicated that amide 3 shared amide 4's oxygen, where in this study, amide 3 clearly prefers amide 2's oxygen. Also, the participation of Asn-3 side chain in solvating the charged carboxylate has never been documented.

The carboxylate binding pocket has a number of unusual properties. As was noted earlier, amide proton exchange is relatively fast for residues 2 and 3 and the side chain NH_2 in the presence of the ligand carboxylate. The calculated structures indicate that the oxygen atoms can occupy a wide variety of conformation space, even being completely out of the pocket, without seriously violating the NOE con-

A

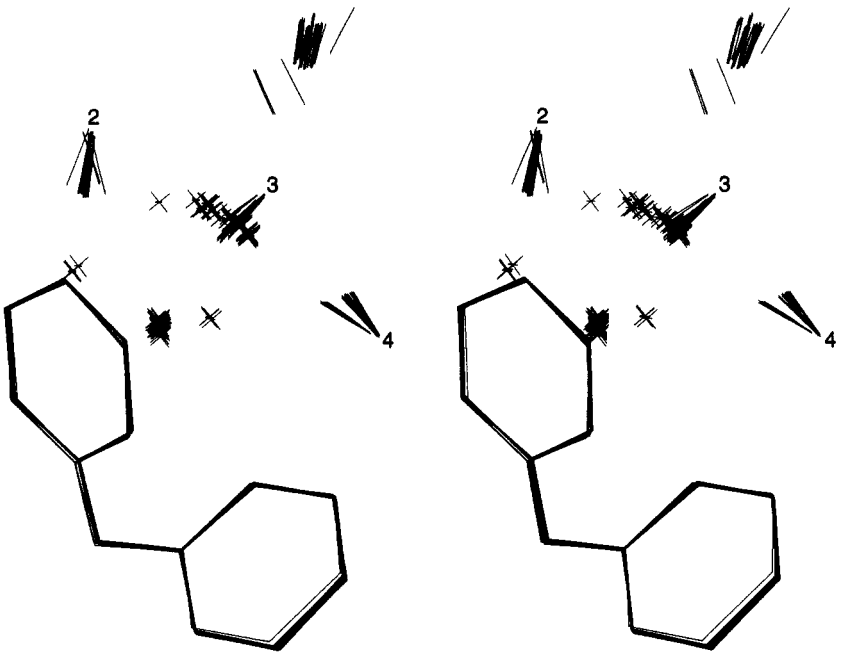

B

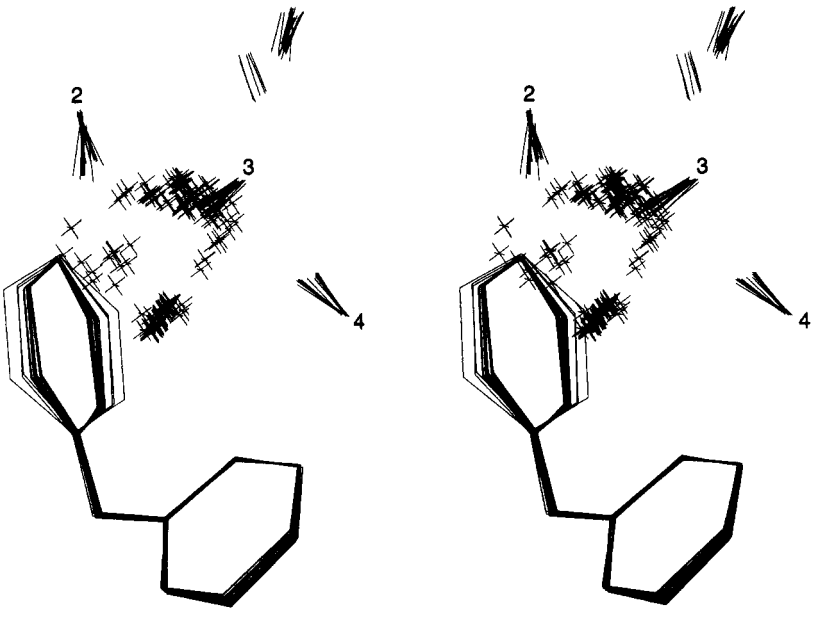

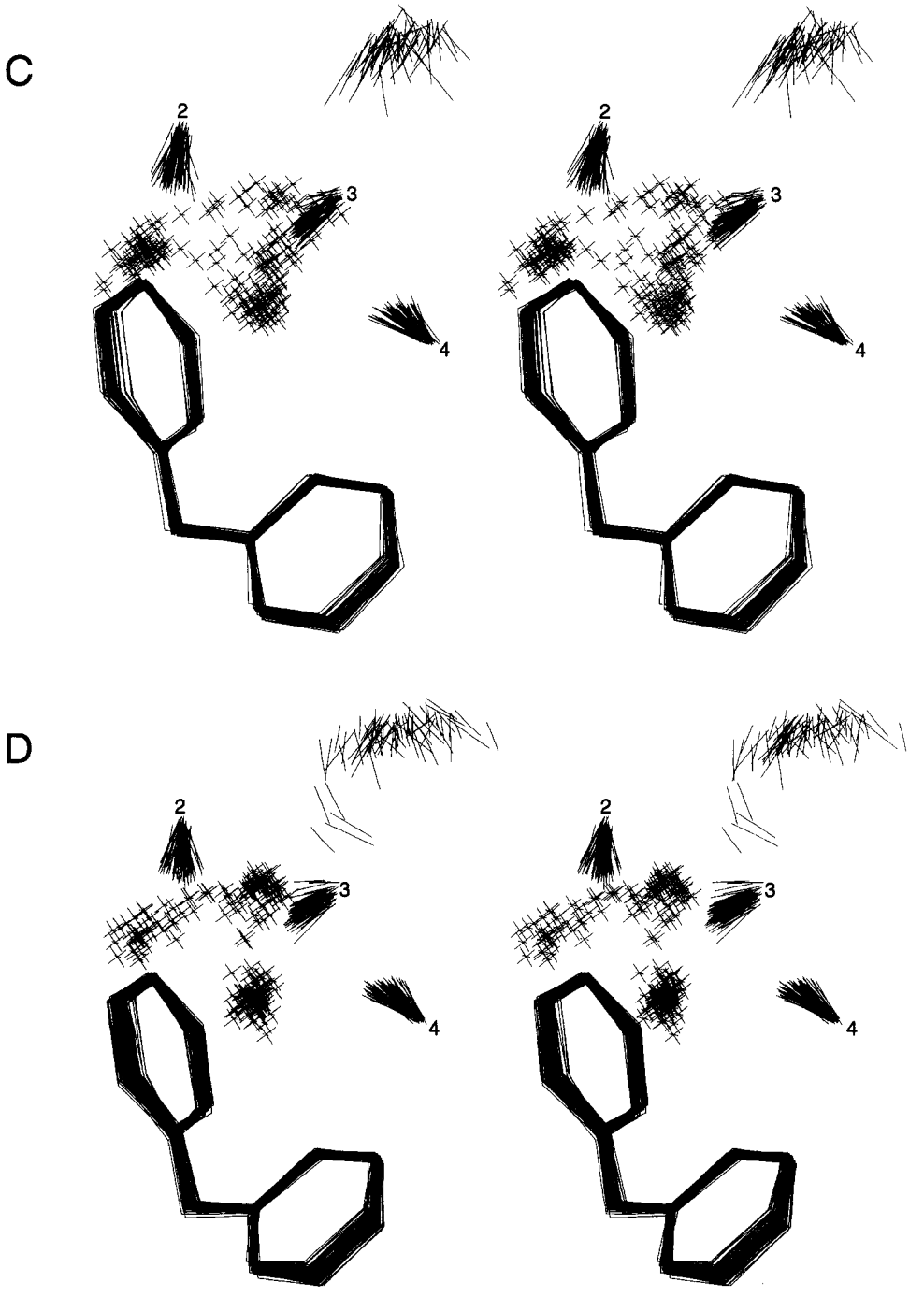

FIGURE 9: Stereodiagrams showing the positions of the dALA-5 carboxylate oxygens with respect to the four amide protons and the aromatic rings 2 and 4 that make up the binding pocket. (A) the binding pocket from segment A of the X-PLOR structures, (B) segment B of the X-PLOR structures, (C) segment A from the CHARMm structures, and (D) segment B from the CHARMm structures. To simplify the illustration, only the atoms directly involved with the carboxylate are drawn. Each binding pocket (A−D) was locally fit to an average using the displayed atoms of the glycopeptide. The NH bonds are labeled with the residue position at the nitrogen end. The bond to the upper right of each diagram represents the Asn-3 $N^{\delta}-N^{\delta}H^{1}$ bond and has its hydrogen closest to the reader. The handful of divergent bonds in this area represent side chains NH's with the amide groups rotated by about 180° (see Figure 4), having their hydrogen oriented away from the reader. All of the oxygens are shown as three-dimensional cross-hatches; because the two oxygen atoms were equivalent in the calculations, no distinction was made between them in the diagram. For the segment A depictions (A) and (C) the six structures with the carboxylates out of the pocket were not drawn.

straints. These data would suggest mobility for the carboxylate. However, the unusually low-field chemical shift of HDPY-2, Asn-3's, and DPYG-4 amide protons (Mueller et al., 1988; Groves et al., 1994b), the heteronuclear NOE observed to the carboxylate carbon (Batta et al., 1992), and the deeply suppressed pK_a (unpublished results, Skelton and Kline) for the ligand carboxylate suggest instead a well-defined singular conformation. The affinity of nonpeptide carboxylates also attests to the importance of this recognition feature (Williams, 1993). The resolution of these seemingly conflicting views of the binding pocket will be a future venture. For this study, the conclusion is that the 23-4N hydrogen bonding network plays a central role in the carboxylate's access to the binding pocket.

A82846B and eremomycin share the same chemical structure except that the former has an additional chlorine

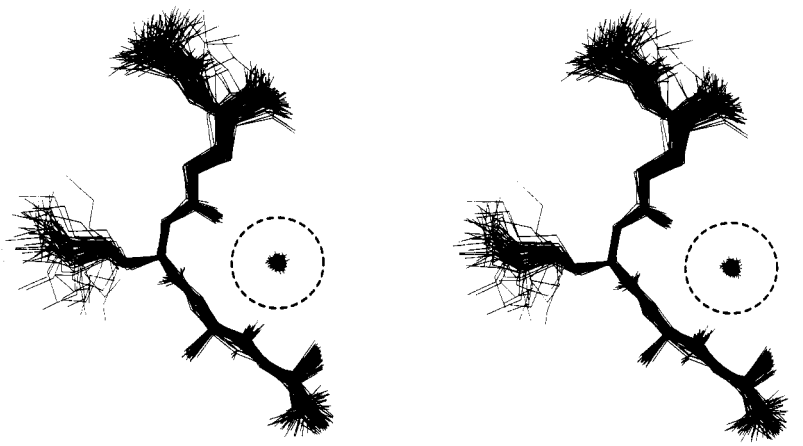

FIGURE 10: Stereodiagram of segment A's peptide ligand with its ring 6 chlorine atoms. All of the heavy atoms of the ligand are shown, while only the chlorine of the glycopeptide is drawn (cross-hatches). Superposition is based on five atoms: the C^{α} of ligand residues 3, 4, and 5, the C^{γ} of GGLU-2 and the ring 6 chlorine. For the ligand the N-terminus is at the top while the C-terminus is at the bottom. For clarity the six structures with carboxylates out of the pocket (see Figure 8) were not drawn. The dashed line shows the approximate van der Waals radius of the chlorine atom. Segment B gives a similar plot and so was not shown.

on ring 6. It has been noted that the presence of this chlorine atom increases its peptide ligand affinity by a factor of 26 (Mackay et al., 1994a). A possible structural basis for the increased affinity can be seen in Figure 10, where the pentapeptide ligand is shown with its ring 6 chlorine atom. The ligand seems to be bent around this atom as if the chlorine were a fulcrum, making numerous contacts with the peptide backbone from GGLU-2 to dALA-4. Replacing the chlorine with a hydrogen would not only drastically shrink the interacting radius but would also withdraw the atom back away from the ligand, reducing its contacts. Evidently the chlorine causes the proper alignments of interaction between the ligand and glycopeptide.

The only published data indicating an interaction for the N-terminal region of the pentapeptide came from an NMR study of aridicin aglycon (Mueller et al., 1989), where intermolecular NOE's were observed for the lysine and glutamate residues. The same is seen for the glycosylated dimer complex of A82846B; specific intermolecular interactions do occur for GGLU-2 and Lys-3. Similar to aridicin aglycon, evidence came from the chemical shifts (supplementary information) and *J*-coupling values of the GGLU-2 β and γ methylene protons. Further, the side chain shifts for the A and B segments (particularly at the β protons) differed significantly from each other. This suggested an interaction with the asymmetrical disaccharides.

Examination of the set of 80 structures indicated that two basic classes of structure occurred, distinguished by the position of their GGLU-2 α-carboxylate. Figure 11 shows examples of both classes for the A and B segments. In one type, the carboxylate lies on top of the HLPY-6 monosaccharide ring; in the other the carboxylate interacts directly with the disaccharide dyad at the dimer interface. To judge the significance of these different classes of structures, several criteria were used: how often in the structures the conformer occurs, potential hydrogen donors to the carboxylate, and agreement with NMR data.

For segment A, 77 of the 80 structures have their carboxylate pointed toward the disaccharide, making the monosaccharide conformer a very minor species. For the B side, however, the monosaccharide conformer is much more significant, claiming 39 structures.

The ionic nature of the carboxylate dictates the expected interactions. In the disaccharide conformers, hydrogen donation consistently occurs from one or both disaccharides, helping to satisfy the charged group. For the monosaccharide conformer, no proton donation is ever seen directly from the glycopeptide; the only donation occurs through water molecules.

The GGLU-2 protons shift between 0.10 and 0.50 ppm from the A to B segment (supplementary information). Comparing the monosaccharide conformers for both A and B, their similarity does not suggest any reason for the disparity in the chemical shifts. However, a comparison for the disaccharide conformers reveals a change from A to B. Figure 12 shows two disaccharide conformers fit together and depicts the difference between the forms. Note the shifting of the carboxylate and the corresponding change for the GGLU-2 side chain. The shift is due to the differences in hydrogen donors from one side of the disaccharide pair to the other. A hydrogen bond is found between the vancosamine C4-CH of the B segment and the GGLU-2 carboxylate of the A segment in 41 of the 77 disaccharide conformers. For the remaining structures, the heavy atoms are still proximal to each other, though the hydrogen is not sufficiently aligned to form a good hydrogen bond. This specific interaction for the A carboxylate with only the B disaccharide is contrasted for the B carboxylate which interacts with both the A and B disaccharides. This accounts for part of the shift to the left in Figure 12; the remainder is due to the change in disaccharide position caused by the 180° rotation. The net result of the carboxylate shift is to change the position of the glutamine side chain relative to the aromatic ring 6. This change with respect to the ring (and its associated ring current) can explain the chemical shift differences between A and B. For all of the above reasons, it is convincing that the GGLU-2 carboxylate is extended, similar to its conformation in the aridicin aglycon complex (Mueller et al., 1989). The carboxylate specifically and predominately interacts with the disaccharide dyad, and the differences in chemical shift for the glutamate protons are due to the side chain shifting with respect to ring 6.

In conclusion, the complex of A82846B and its cell-wall pentapeptide form an asymmetrical dimer similar to that seen

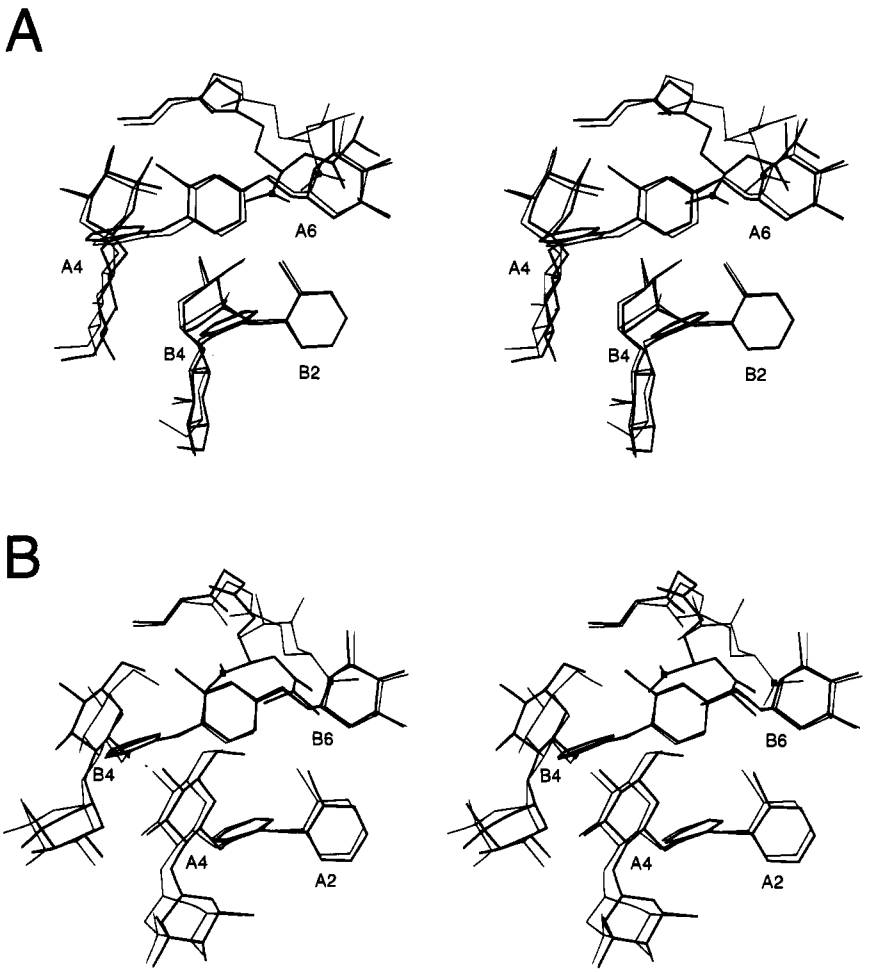

FIGURE 11: Stereodiagram depicting the two conformers seen for the carboxylate of GGLU-2. (A) Interactions of segment A's carboxylate. (B) Segment B's carboxylate. A subset of the heavy atoms are drawn from four of the 80 CHARMm structures. The carbon atoms of the ligand carboxylate are marked. The thick line respresents the "disaccharide" conformer while the thin line represents the "monosaccharide" conformer (see text). Side chains for the glycopeptide are labeled by segment and residue position. The superposition was done using the ring atoms from the four aromatic rings and the monosaccharide shown in each picture.

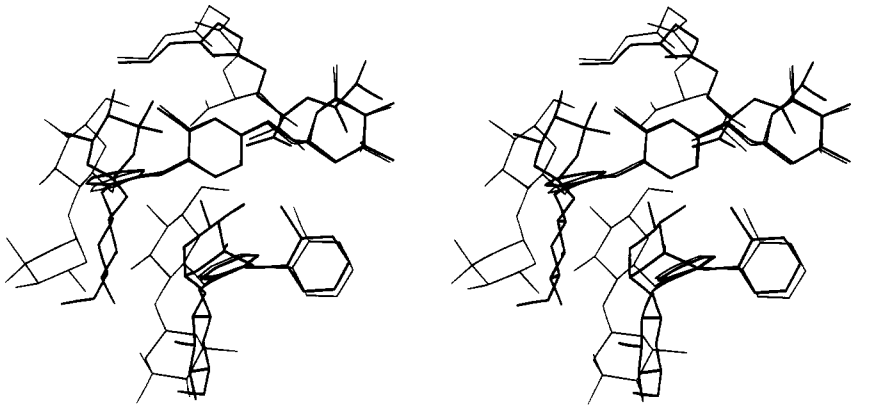

FIGURE 12: Comparison of the disaccharide conformers for the GGLU-2 carboxylate from segments A (thick) and B (thin). The disaccharide conformers from Figure 10 A and B were superimposed using the same atoms and orientation. The carbon atoms of the carboxylate are marked.

for eremomycin and its (pyrrole-2-carboxylate) ligand (Groves et al., 1994a). Proton assignments for this quaternary complex were achieved by homonuclear two-dimensional methods, which allowed the collection of 683 experimental constraints. Structure calculations with both X-PLOR and CHARMm programs indicated that the full force field opens up additional allowed conformational space not seen in the X-PLOR calculations. Carboxylate binding of the terminal dALA-5 occurs by a series of four hydrogen bonds; backbone amide protons from residues 2 and 3 engage one oxygen, while the backbone amide from residue 4 and the side chain amide from Asn-3 share the remaining oxygen. The GGLU-2 and Lys-3 from the pentapeptide have a defined and unique interaction with the glycopeptide dimer. The Lys-3 amide proton is hydrogen bonded to the C-terminal carboxylate of A82846B. The carboxylate of GGLU-2 hydrogen bonds with the asymmetric disaccharide dyad, producing different ligand conformations for the two halves

of the dimer. This difference in conformation is highlighted in the chemical shift values of the glutamate side chain and is caused principally by the ring current field of HLPY-6.

ACKNOWLEDGMENT

A82846B and the pentapeptide were graciously provided by Dr. Richard Thompson. Dr. Bernard Brooks (NIH) provided valuable guidance on CHARMm. Drs. Norris Allen, Robin Cooper, Ann Hunt, Thalia Nicas, and Richard Thompson all provided the authors with useful information on glycopeptide antibiotics and were helpful in evaluating this manuscript.

SUPPORTING INFORMATION AVAILABLE

A list of the proton chemical shifts for the A82846B–pentapeptide complex and a list of the individual distance constraints used in the structure calculations as well as the Residue Topology File (CHARMm or X-PLOR format) necessary for calculating the structures of A82846B (34 pages). Ordering information is given on any current masthead page.

REFERENCES

Arthur, M., & Courvalin, P. (1993) *Antimicrob. Agents Chemother. 37*, 1563–1571.
Batta, Gy., Kövér, K. E., Székely, Z., & Sztaricskai, F. (1992) *J. Am. Chem. Soc. 114*, 2757–2758.
Bax, A., & Subramanian, S. (1986) *J. Magn. Reson. 67*, 565–569.
Beauregard, D. A., Williams, D. H., Gwynn, M. N., & Knowles, D. J. C. (1995) *Antimicrob. Agents Chemother. 39*, 781–785.
Bodenhausen, G., Kogler, H., & Ernst, R. R. (1984) *J. Magn. Reson. 58*, 370–388.
Braunschweiler, L., & Ernst, R. R. (1983) *J. Magn. Reson. 53*, 521–528.
Brooks, B. R., Bruccoleri, R. E., Olafson, B. D., States, D. J., Swaminathan, S., & Karplus, M. (1983) *J. Comput. Chem. 4*, 187–217.
Brünger, A. T. (1992) *X-PLOR Version 3.1, A System for X-Ray Crystallography and NMR*, Yale University Press, New Haven, CT.
Clore, G. M., & Gorenborn, A. M. (1993) *NMR of Proteins*, pp 1–27, CRC Press, Ann Arbor, MI.
Fejzo, J., Westler, W. M., & Markley, J. L. (1990) *J. Am. Chem. Soc. 112*, 2574–2577.
Fesik, S. W., Armitage, I. M., Ellestad, G. A. & McGahren, W. J. (1984) *Mol. Pharmacol. 25*, 281–286.
Fesik, S. W., O'Donnell, T. J., Gampe, R. T., Jr., & Olejniczak, E. T. (1986) *J. Am. Chem. Soc. 108*, 3165–3170.
Gerhard, U., Mackay, J. P., Maplestone, R. A., & Williams, D. H. (1993) *J. Am. Chem. Soc. 115*, 232–237.
Groves, P., Searle, M. S., Mackay, J. P., & Williams, D. H. (1994a) *Structure 2*, 747–754.
Groves, P., Searle, M. S., Westwell, M. S., & Williams, D. H. (1994b) *J. Chem. Soc., Chem. Commun.*, 1519–1520.
Hunt, A. H., Occolowitz, J. L., Debono, M., & Molloy, R. M. (1988) 28th Interscience Conference on Antimicrobial Agents and Chemotherapy, Abstract #976.
Kannan, R., Harris, C. M., Harris, T. M., Waltho, J. P., Skelton, N. J., & Williams, D. H. (1988) *J. Am. Chem. Soc. 110*, 2946–2953.
Mackay, J. P., Gerhard, U., Beauregard, D. A., Maplestone, R. A., & Williams, D. H. (1994a) *J. Am. Chem. Soc. 116*, 4573–4580.
Mackay, J. P., Gerhard, U., Beauregard, D. A., Westwell, M. S., Searle, M. S., & Williams, D. H. (1994b) *J. Am. Chem. Soc. 116*, 4581–4590.
McCormick, M. H., Stark, W. M., Pittenger, G. E., Pittenger, R. C., & McGuire, J. M. (1956) *Antiobiot. Annu. 1955–1956*, 601–611.
Mueller, L., Heald, S. L., Hempel, J. C., & Jeffs, P. W. (1989) *J. Am. Chem. Soc. 111*, 496–505.
Nagarajan, R. (1993) *Glycopeptide Antibiotics*, Marcel Dekker, New York.
Nagarajan, R., Berry, D. M., Hunt, A. H., Occolowitz, J. L., & Schabel, A. A. (1988) *J. Org. Chem. 54*, 983–986.
Nagarajan, R., Berry, D. M., & Schabel, A. A. (1989) *J. Antibiot. 42*, 1438–1440.
Nieto, M., & Perkins, H. R. (1971) *Biochem. J. 123*, 773–787.
Rance, M. (1987) *J. Magn. Reson. 74*, 557–564.
Rance, M., Sorensen, O. W., Bodenhausen, G., Wagner, G., Ernst, R. R., & Wüthrich, K. (1983) *Biochem. Biophys. Res. Commun. 117*, 479–485.
Rucker, S. P., & Shaka, A. J. (1989) *Mol. Phys. 68*, 509–517.
Sheldrick, G. M., Jones, P. G., Kennard, O., Williams, D. H., & Smith, G. A. (1978) *Nature 271*, 223–225.
Sheldrick, G. M., Paulus, E., Vértesy, L., & Hahn, F. (1995) *Acta Crystallogr. B51*, 89–98.
Wagner, G., & Wüthrich, K. (1982) *J. Mol. Biol. 160*, 343–361.
Waltho, J. P., & Williams, D. H. (1989) *J. Am. Chem. Soc. 111*, 2475–2480.
Waltho, J. P., Williams, D. H., Stone, D. J. M., & Skelton, N. J. (1988) *J. Am. Chem. Soc. 100*, 5638–5643.
Wilhelm, M. P. (1991) *Mayo Clin. Proc. 66*, 1165–1170.
Williams, D. H. (1984) *Acc. Chem. Res. 17*, 364–369.
Williams, D. H., & Butcher, D. W. (1981) *J. Am. Chem. Soc. 103*, 5697–5700.
Williams, D. H., Williamson, M. P., Butcher, D. W., & Hammond, S. J. (1983) *J. Am. Chem. Soc. 105*, 1332–1339.
Williams, D. H., Searle, M. S., Mackay, J. P., Gerhard, U., & Maplestone, R. A. (1993) *Proc. Natl. Acad. Sci. U.S.A. 90*, 1172–1178.
Williamson, M. P., & Williams, D. H. (1985) *J. Chem. Soc. Perkin. Trans. 1*, 949–956.
Williamson, M. P., Williams, D. H., & Hammond, S. J. (1984) *Tetrahedron 40*, 569–577.
Wright, G. D., & Walsh, C. T. (1992) *Acc. Chem. Res. 25*, 468–473.
Wüthrich, K. (1986) *NMR of Proteins and Nucleic Acids*, Wiley-Interscience, New York.

BI9507185